Journal of Physics: Conference Series

OPEN ACCESS

Investigation of the strain-sensitive superconducting transition of $BaFe_{1.8}Co_{0.2}As_2$ thin films utilizing piezoelectric substrates

To cite this article: S Trommler *et al* 2014 *J. Phys.: Conf. Ser.* **507** 012049

View the article online for updates and enhancements.

Related content

- Reversible shift in the superconducting transition for La1.85Sr0.15CuO4 and BaFe1.8Co0.2As2 using piezoelectric substrates
S Trommler, R Hühne, K Iida et al.
- TSEE from MgO Single Crystal Physically Processed
Jose Fernando, Diniz Chubachi, Toru Kakiage et al.
- TSEE from MgO Single Crystals Introduced by Cleaving
T. Seiyama, K. Kawabata and S. Okuda

This content was downloaded from IP address 194.95.158.35 on 04/06/2018 at 11:17

Journal of Physics: Conference Series **507** (2014) 012049 doi:10.1088/1742-6596/507/1/012049

Investigation of the strain-sensitive superconducting transition of $BaFe_{1.8}Co_{0.2}As_2$ thin films utilizing piezoelectric substrates.

S. Trommler[1], J. Hänisch, K. Iida, F. Kurth, L. Schultz[1] and B. Holzapfel[2], R. Hühne

IFW Dresden, Institute for Metallic Materials, P.O. Box 270116, 01171 Dresden, Germany
[1] Technische Universität Dresden, Department of Physics, Institute for Physics of Solids, 01062 Dresden, Germany
[2] TU Bergakademie Freiberg, 09596 Freiberg, Germany

E-mail: s.trommler@ifw-dresden.de

Abstract. The preparation of biaxially textured $BaFe_{1.8}Co_{0.2}As_2$ thin films has been optimized on MgO single crystals and transfered to piezoelectric (001) $Pb(Mg_{1/3}Nb_{2/3})_{0.72}Ti_{0.28}O_3$ substrates. By utilizing the inverse piezoelectric effect the lattice parameter of these substrates can be controlled applying an electric field, leading to a induction of biaxial strain into the superconducting layer. High electric fields were used to achieve a total strain of up to 0.05% at low temperatures. A sharpening of the resistive transition and a shift of about 0.6 K to higher temperatures was found at a compressive strain of 0.035%.

The interplay of structural properties and intrinsic parameters is widely used to study superconducting materials [1, 2, 3]. Traditionally, the lattice mismatch between substrate and film material is used to generate statically strained films. Simultaneously, relaxation effects lead to the implementation of defects during the growth process, which changes the microstructure and thus affect thin film properties like the critical current density and pinning mechanisms. Therefore, the suitability of this method is strongly limited, since strain-driven effects are hard to separate from preparation related changes.

Alternatively, the application of single crystalline piezoelectric $Pb(Mg_{1/3}Nb_{2/3})_{0.72}Ti_{0.28}O_3$ (PMN-PT) substrates has been demonstrated to provide the control of reversible and dynamic strain in thin functional films [4, 5, 6, 7] and thus give the opportunity to study the strain sensitivity of microstructure related properties in superconducting thin films. However, the adaptation of this approach to pnictides requires the application of suitable buffer layers to prevent any oxidation. In this paper we report on the utilization of an Fe/MgO buffer to the model system $BaFe_{1.8}Co_{0.2}As_2$ (Ba-122) which might be also suitable for other Fe based superconductors.

The samples were prepared in ultra-high vacuum (10^{-9} mbar) using pulsed laser deposition and stoichiometric targets. A detailed description of the target and sample preparation was published previously [8, 9, 10]. During deposition, the film evolution is monitored with reflection high energy electron diffraction (RHEED), whereas for structural characterization x-ray $\theta/2\theta$ scans and pole figure measurements in a four circle goniometer were performed. For the application of dynamic strain the sample was split into 1 mm wide stripes and contacted at

Content from this work may be used under the terms of the Creative Commons Attribution 3.0 licence. Any further distribution of this work must maintain attribution to the author(s) and the title of the work, journal citation and DOI.
Published under licence by IOP Publishing Ltd

the Au/NiCr bottom electrode. The top electrode is provided by the film itself and connected to ground level to avoid any field effects. For electrical characterization contacts were attached to the sample surface with silver glue in a four-probe geometry. The PMN-PT was poled with 10 kV/cm at room temperature (RT) and subsequently cooled down at 6.6 kV/cm. The resistive transition was recorded with 10 μA and 1 K/min in a Physical Property Measurement System (Quantum Design). The critical temperature is defined at a criterion of 90% of the normal state resistance, noted here as $T_{c,90}$.

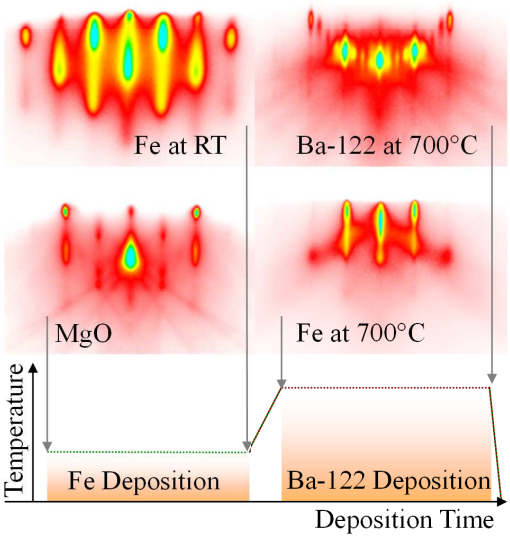

Figure 1. RHEED pattern of selected deposition steps for the preparation of a Ba-122/Fe bilayer on MgO single crystal.

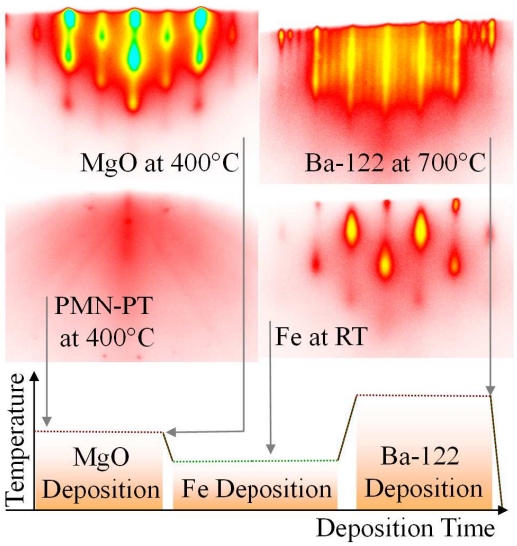

Figure 2. RHEED pattern of selected deposition steps for the preparation of a Ba-122/Fe bilayer on MgO buffered PMN-PT.

In the first step the film preparation was optimized on MgO single crystalline substrates (MgO SC). To improve the epitaxial growth of Ba-122, an artificial Fe buffer layer was introduced resulting in a clean and coherent Ba-122/Fe interface [9, 11]. A typical deposition sequence on MgO with the corresponding RHEED images is given in fig. 1. The MgO diffraction pattern reveals sharp peaks and Kikuchi lines, typical for polished single crystalline substrates. The diffraction pattern of 20 nm Fe, deposited at RT, originates from the transmission of textured 3D structures, indicating island growth. The peaks broadening arises from a a small grain size, which is due to the small lattice coherence. During the heating ramp the Fe diffraction pattern changes drastically, which can be attributed to recrystallization effects leading to a peak sharpening. The arrangement on Laue circles and the occurrence of Kikuchi lines indicate a reduction of the surface roughness and an enhancement of the lattice coherence. Directly after approaching the desired temperature, 50 nm Ba-122 are deposited. The distinct arrangement of the diffraction peaks on Laue circle evidences a 2D-like surface, whereas additional intermediate peaks reveal the formation of a surface reconstruction, which was also observed for previous films [12].

A similar layer architecture was applied to PMN-PT substrates (fig. 2). The low intensity of the diffraction peaks for PMN-PT arises from a higher mosaicity of the crystal. However, the peaks are arranged on Laue circles, indicating a smooth surface. 20 nm MgO are deposited at 400 °C since a diffusion barrier is required to avoid any oxidation of the Ba-122/Fe bilayer. The diffraction pattern is similar to a MgO SC, but with broadened peaks. After cooling down to RT iron is deposited, showing an similar diffraction pattern as the corresponding Fe on MgO SC. In contrast, no significant change is observed during ramping up the temperature. This

can be attributed to the transfer of the substrate mosaicity into the subsequent layers, avoiding recrystallization effects. Finally, the Ba-122 film exhibits vertically elongated peaks, which is typical for the transition between layer and island growth. Additional lines connected to a surface reconstruction are observed, which indicate similar surface properties on both substrates.

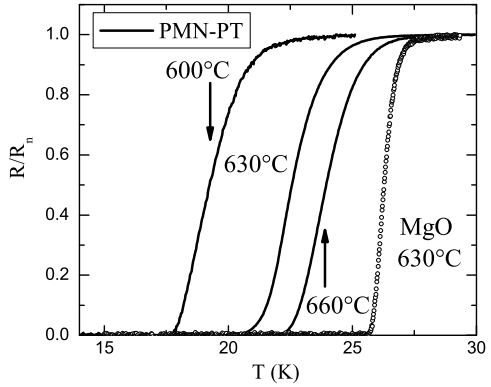

Figure 3. Resistive transition of Ba-122/Fe bilayers on MgO-buffered PMN-PT for different temperatures in comparison to a Ba-122/Fe bilayer on MgO single crystal.

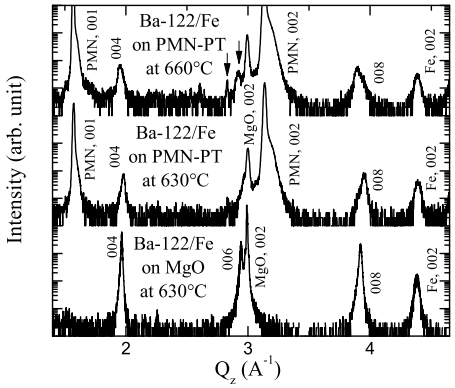

Figure 4. $\theta/2\theta$ scans of Ba-122/Fe bilayers on MgO-buffered PMN-PT for two temperatures in comparison to a Ba-122/Fe bilayer on MgO single crystal.

In general, we observe a a higher T_c with increasing deposition temperature of Ba-122. For MgO substrates the optimal deposition temperature was found to be 630 °C, with a maximum $T_{c,90}$ of 26.9 K and a very small transition width of $\Delta T = 1$ K (see fig. 3). A similar dependency is found for films on PMN-PT substrates, with an optimal deposition temperature of 660 °C resulting in $T_{c,90} = 25.5$ K. The broadening of the resistive transition with $\Delta T = 2.6$ K is found to be independent from the resulting $T_{c,90}$ and might be due to the higher defect density in films on PMN-PT, as discussed above.

Standard $\theta/2\theta$ scans (fig. 4) prove pure c-axis growth of Ba-122 on both MgO and PMN-PT, and the known epitaxial relationship was confirmed by pole figure measurements. With increasing deposition temperature, additional peaks appear (arrows), which are also present for just heated reference substrates and originate from a temperature-induced decomposition of the substrate. To avoid any degradation of the piezoelectric performance of the PMN-PT crystal, the strain experiments were carried out on films grown at 600 °C with $T_{c,90} = 20.5$ K. After poling and cooling down the sample to 10 K the resistive transition was measured for different electric fields (fig. 5). According to previous studies at 20 K [7], the substrate provides about a linear strain of $\epsilon_{ab} = 0.017\%$ for 13.3 kV/cm. Due to the polarity of the substrate, a positive field leads to compressive strain, whereas a negative field induces tensile strain.

An increasing biaxial compression results in a shift of the resistive transition to higher temperatures with a total shift of $T_{c,90}$ of about 0.6 K for $\epsilon_{ab} = 0.035\%$. To illustrate the strain sensitivity of the whole transition slope, a criterion-dependent temperature shift can be defined as $\Delta T(p)$ at the resistance criterion R_p, where $p = R_p/R_{30K}$. Exemplary, this is displayed for $\Delta E = 26.6$ kV/cm in the inset of fig. 5. For all slopes we find an increasing $\Delta T(\epsilon_{ab})$ with decreasing p. This behavior can be explained taking into account, that the shape of the resistive transition is influenced by different mechanisms, as pinning, thermal activation or fluctuations, which generally have different strain sensitivities. $T_{c,90}$ as well as T_{irr} is highlighted in the inset, where T_{irr} is defined for $p = 10^{-2}$ and exhibits roughly twice the temperature shift compared to $T_{c,90}$.

To get deeper insight, we fitted the slopes according to the vortex-glass theory, where

$R \propto (T - T_g)^{\alpha}$ [13]. The total shift in dependence of the applied electric field is displayed in fig. 6. For compressive strain we find a linear behavior for both T_g and $T_{c,90}$, where T_g represents the broadening of the resistive transition close to zero resistance (see the inset of fig. 6). In contrast, for tensile strain we observe almost no change in $T_{c,90}$ but a strong broadening of the transition, which might be connected to the formation of cracks. This would lead to a non-uniform strain transfer into the superconducting layer, where the lattice keeps almost unstrained. With increasing tension the cracks will open and reduce the number of superconducting current paths resulting in an increased local current density, which thus increases the resistance and broadens the slope. Due to the low thermal expansion coefficient of PMN-PT [14] the film is tensile-strained at low temperature compared to RT. Therefore, any crack formation may be closed and not noticeable at RT.

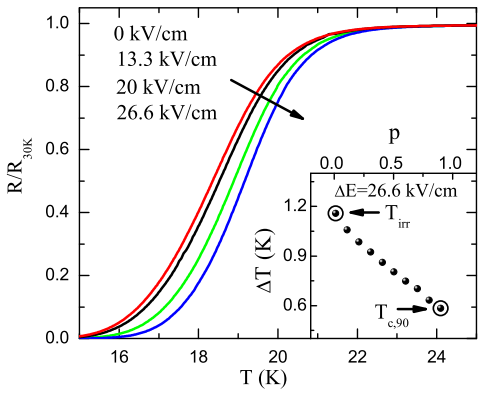

Figure 5. Resistive transition of a Ba-122/Fe bilayer on MgO-buffered PMN-PT for different electric fields, resulting in compressive strain. The inset displays the shift of the transition in dependency of R_p.

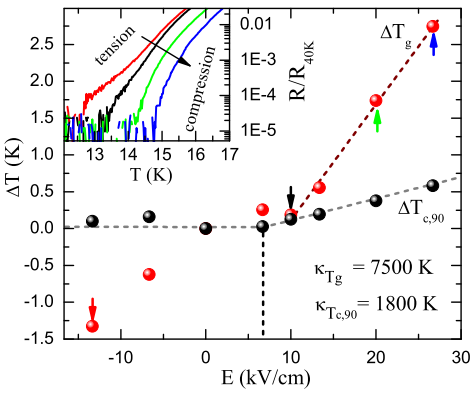

Figure 6. Strain-induced shift of $T_{c,90}$ and T_g. The inset displays the curvature change of the transition close to zero resistance with increasing compressive strain (fields are marked by arrows).

Based on the total differential of the specific resistivity, the strain sensitivity is defined as $\kappa = \Delta T/\epsilon_{ab}$. At compressive strain, the best fit yields a strain sensitivity of 1800 K for $T_{c,90}$ and 7500 K for T_g, respectively. The 4 times larger strain sensitivity of T_g compared to $T_{c,90}$ is related to a transition sharpening with increasing in-plane compression. Therefore, the linear field dependency for T_g has to deviate at high electric fields due to the limited transition width.

[1] L. Gao, Y. Y. Xue, F. Chen, Q. Xiong, R. L. Meng, D. Ramirez et al., Phys. Rev. B **50** (1994), 4260.
[2] H. Takahashi, K. Igawa, K. Arii, Y. Kamihara, M. Hirano and H. Hosono, Nature **453** (2008), 376.
[3] S. Medvedev, T. M. McQueen, I. A. Troyan, T. Palasyuk et al., Nature Materials **8** (2009), 630.
[4] R. Hühne, D. Okai, K. Dörr, S. Trommler, A. Herklotz et al., Supercond. Sci. Technol. **21** (2008), 075020.
[5] A. D. Rata, A. Herklotz, K. Nenkov, L. Schultz, and K. Dörr, Phys. Rev. Lett. **100** (2008), 076401.
[6] A. Herklotz, A. D. Rata, L. Schultz, and K. Dörr, Phys. Rev. B **79** (2009), 092409.
[7] S. Trommler, R. Hühne, K. Iida, P. Pahlke, S. Haindl, L. Schultz et al., New J. Phys. **12** (2010), 103030.
[8] F. Kurth, K. Iida, S. Trommler, J. Hänisch, K. Nenkov et al., Supercond. Sci. Technol. **26** (2013), 025014.
[9] K. Iida, S. Haindl, T. Thersleff, J. Hänisch, F. Kurth et al., Appl. Phys. Lett. **97** (2010), 172507.
[10] S. Trommler, J. Hänisch, V. Matias, R.Hühne, E. Reich et al., Supercond. Sci. Technol., **25** (2012), 084019.
[11] T. Thersleff, K. Iida, S. Haindl, M. Kidszun, D. Pohl et al., Appl. Phys. Lett. **97** (2010), 022506.
[12] K. Iida, J. Hänisch, S. Trommler, S. Haindl, F. Kurth et al., Supercond. Sci. Technol., **24** (2011), 125009.
[13] D.S. Fisher, M.P.A. Fisher and D.A. Huse, Phys. Rev. B **43** (1991), 130159.
[14] H.W. King, S.H. Ferguson, D.F. Waechter and S.E. Prasad, Proceedings of ICONS (2002).